MAGNETIC RESONANCE IN CHEMISTRY
Magn. Reson. Chem. 2000; **38**: 604–614

Triple proton transfer in crystalline 3,5-dibromo-1*H*-1,2,4-triazole and 3,5-dichloro-1*H*-1,2,4-triazole studied by variable-temperature ^{15}N NMR and *ab initio* calculations†

María Angeles García,[1] Concepción López,[1] Olaf Peters,[1] Rosa M. Claramunt,[1]* Oliver Klein,[2] David Schagen,[2] Hans-Heinrich Limbach,[2] Concepción Foces-Foces[3] and José Elguero[4]

[1] Departamento de Química Orgánica y Biología, Facultad de Ciencias, UNED, Senda del Rey 9, E-28040 Madrid, Spain
[2] Fachbereich Biologie, Chemie und Pharmazie, Institut für Chemie, Freie Universität Berlin, Takustrasse 3, D-14195 Berlin, Germany
[3] Departamento de Cristalografía, Instituto de Química-Física Rocasolano, CSIC, Serrano 119, E-28006 Madrid, Spain
[4] Instituto de Química Médica, Centro de Química Orgánica Manuel Lora-Tamayo, CSIC, Juan de la Cierva 3, E-28006 Madrid, Spain

Received 14 January 2000; revised 22 February 2000; accepted 22 February 2000

ABSTRACT: Results are reported of variable-temperature ^{15}N cross-polarization magic angle spinning (CP/MAS) NMR experiments performed on [$^{15}N_2$]-labelled polycrystalline 3,5-dibromo-1*H*-1,2,4-triazole (**2b**) and 3,5-dichloro-1*H*-1,2,4-triazole (**3b**), the synthesis of which is also described. According to the crystal structures these compounds form cyclic trimers in the solid state. The molecular and hydrogen bond structures were compared with those derived from *ab initio* calculations. The ^{15}N CP/MAS NMR spectra show temperature-dependent lineshapes which were analysed in terms of near-degenerate triple proton transfer processes. The equilibrium constants are slightly different from unity as observed by high-temperature line splittings. The populations of the two quasi-degenerate tautomers were calculated from the internal angles at N1 and N2 and compared with those obtained from solid-state NMR; both methods agree fairly well. By lineshape analysis rate constants of the triple proton transfer processes were obtained at different temperatures. The proton transfer kinetics of **2b** and **3b** were compared with those of 3,5-dimethylpyrazole, 4-nitropyrazole and 4-bromopyrazole, studied previously, which also form cyclic trimers in the solid state, exhibiting more or less concerted, degenerate triple proton transfer processes proceeding by tunnelling at low temperatures. It is shown that the triazoles behave in a similar way to the pyrazoles. The barrier heights of the triple proton transfer increase monotonically with the distance between the two nitrogen atoms involved in the proton transfer. It is shown that the intrinsic nitrogen chemical shifts are related to the N···H distances. Copyright © 2000 John Wiley & Sons, Ltd.

KEYWORDS: NMR; cross-polarization magic angle spinning NMR; 1,2,4-triazoles, solid state; triple proton transfer; *ab initio* calculations

INTRODUCTION

Whereas the solid-state proton transfer of pyrazoles has been well established using solid-state NMR spectroscopy, little is known about the behaviour of the corresponding 1,2,4-triazoles (Fig. 1).

In principle, this class of molecules can form two non-equivalent tautomers with a proton either localized on N1 (1*H* tautomer) or N4 (4*H* tautomer). As the energy difference between the two tautomers is very large,[1] only the 1*H* tautomer needs to be considered under normal conditions. As pyrazoles, the triazoles are at the same time hydrogen bond donors (HBD) and hydrogen bond acceptors (HBA). When N4 nitrogen acts as HBA a '2-azaimidazole' structure results, leading to more or less linear hydrogen-bonded chains (catemers) as depicted in Fig. 1. On the other hand, when the N2 nitrogen acts as HBA an 'azapyrazole' structure is obtained which forms either zig-zag chains or cyclic hydrogen-bonded associates, as depicted in Fig. 1 for the cyclic trimer. In the crystalline state the parent compound **1** forms catemers, as has been found by several workers using x-ray crystallography and neutron diffraction.[2–5] Up to now, zig-zag chains have not been observed in the case of triazoles. By contrast, cyclic trimers have been recently observed by x-ray crystallography in the cases of 3,5-dibromo- (**2a**) and 3,5-dichloro-1*H*-1,2,4-triazole (**3a**).[6–8] These trimers are very similar to that formed

† This paper is dedicated to Professor Dr Harald Günther on the occasion of his 65th birthday.

* *Correspondence to*: R. M. Claramunt, Departamento de Química Orgánica y Biología, Facultad de Ciencias, UNED, Senda del Rey 9, E-28040 Madrid, Spain; e-mail: rclaramunt@ccia.uned.es
Contract/grant sponsor: DGICYT; *Contract/grant number*: PB96-0001-C03.
Contract/grant sponsor: Comunidad de Madrid; *Contract/grant number*: 07N/0001/1999.
Contract/grant sponsor: Deutsche Forschungsgemeinschaft.
Contract/grant sponsor: Fonds der Chemischen Industrie.

by 3,5-dimethylpyrazole (**4**) (dmpz),[9,10] 4-nitropyrazole (**5**) (4no2pz) and 4-bromopyrazole (**6**) (4brpz)[11] which exhibit degenerate triple proton transfer in the solid state as indicated in Fig. 1.

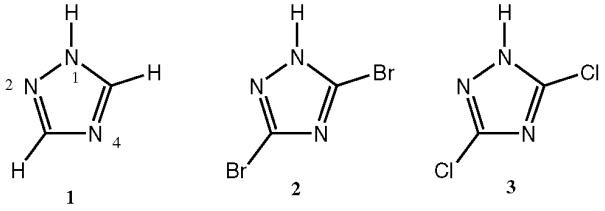

1 **2** **3**

a, unlabelled compounds; **b**, $^{15}N_2$-labelled compounds (N1, N2)

Whereas the reported x-ray structures of **2a** and **3a** indicated localized NH protons, the endocyclic angles at the nitrogen atoms seemed to be indicative of proton disorder. In order to resolve this contradiction we, decided to re-examine this problem using dynamic solid-state ^{15}N NMR spectroscopy of the ^{15}N-labelled compounds **2b** and **3b**. Some preliminary results indicated interesting temperature-dependent spectral phenomena.[12] The synthesis of **2b** and **3b** and the results of the NMR study are reported in this paper, including the thermodynamic and kinetic parameters of the triple proton transfer processes according to Fig. 1, obtained by lineshape analysis. The kinetic results are compared with those obtained previously[9–11] for **4**, **5** and **6**. Moreover, the structures of the triazole trimers were calculated using *ab initio* methods and compared with the crystallographic data.

EXPERIMENTAL

Syntheses

Melting-points were determined in a microscope hot-stage apparatus and on a Seiko DSC 220C instrument with a scanning rate of 2 °C min^{-1}. Commercial [$^{15}N_2$]hydrazine sulfate (95% ^{15}N) was purchased from Chemotrade.

Synthesis of 1*H*-[$^{15}N_2$]1,2,4-triazole (1b). In a 100 ml round-bottomed flask provided with a refrigerant and a magnetic stirrer were placed 0.774 g (0.0077 mol) of well powdered potassium hydrogencarbonate, 1 g (0.0076 mol) of [$^{15}N_2$]hydrazine sulfate, 0.405 g (0.005 mol) of *s*-triazine and 40 ml of ethanol (water-free). This mixture was boiled for 18 h under reflux. After cooling to room temperature, 90 ml of diethyl ether were added to the colourless reaction mixture and the salts were filtered off. The ethanol–ether solution was removed under reduced pressure. The residue was recrystallized from chloroform (m.p. 120 °C, lit.[13] m.p. 120–121 °C). The total yield of 1*H*-[$^{15}N_2$]1,2,4-triazole (**1b**) was 0.414 g (78%); lit.[13] yield 35%.

Synthesis of 3,5-dibromo-1*H*-[$^{15}N_2$]1,2,4-triazole (2b). A solution of 0.414 g (0.0058 mol) of 1*H*-[$^{15}N_2$]1,2,4-triazole (**1b**) in 10 ml of water was treated with 1.4 g of potassium hydrogencarbonate and then was heated to 80 °C, and with stirring 0.66 ml (0.013 mol) of bromine in an aqueous solution of potassium bromide (0.5 g of KBr in 1 ml of water) was added. The reaction mixture was brought to ebullition to eliminate the excess of bromine. After cooling, the reaction mixture was acidified with hydrochloric acid. The precipitate was filtered off and washed with cold water. Compound **2b** was crystallized from water (m.p. by DSC 203.9 °C; lit.[14] m.p. 210–211 °C); yield 1.32 g (99%).

Synthesis of 3,5-dichloro-1*H*-[$^{15}N_2$]1,2,4-triazole (3b). A 0.5 g (0.0022 mol) amount of 3,5-dibromo-1*H*-[15N$_2$]1,2,4-triazole (**2b**), 1.27 g of sodium chloride and 25 ml of concentrated hydrochloric acid were mixed in a 250 ml Berghof high-pressure autoclave (maximum working pressure 100 atm) and heated at 160 °C for 4 h. After cooling, the reaction mixture was dropped into 5 ml of water and neutralized with sodium hydroxide and evaporated to dryness. The residue was extracted

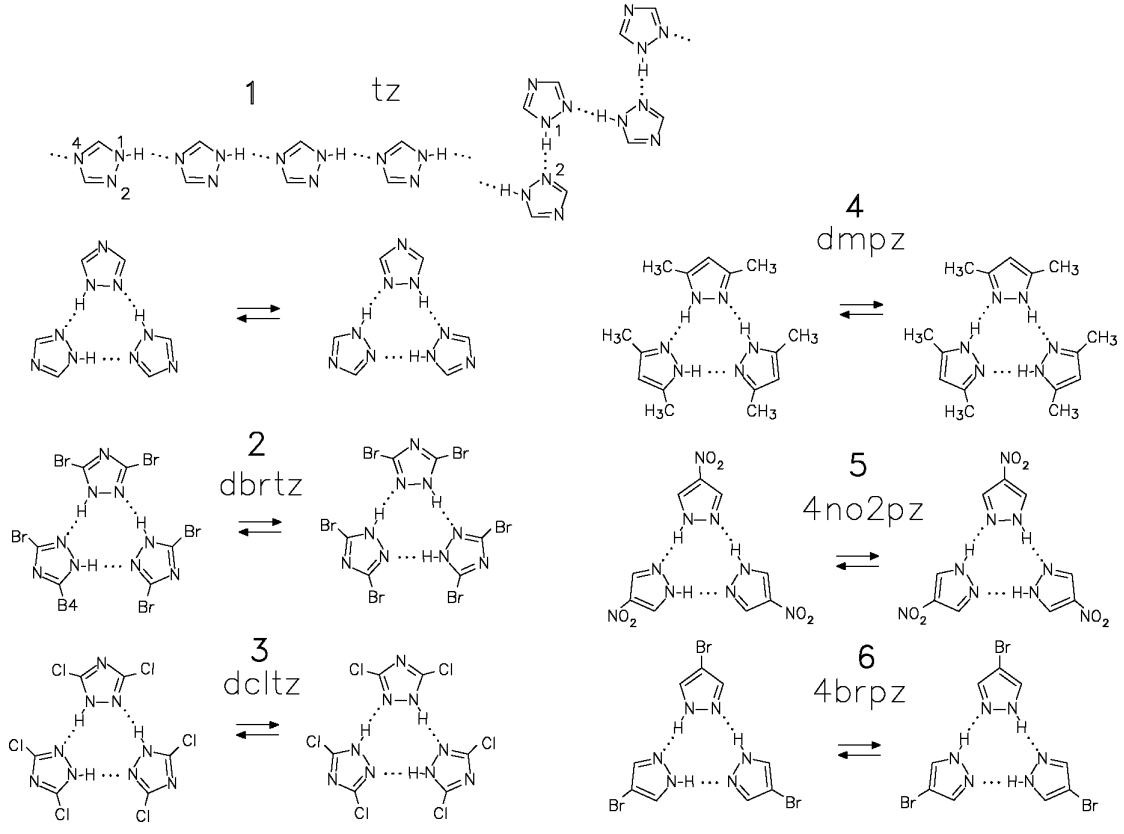

Figure 1. 1*H*-1,2,4-Triazole (**1**) behaving like an imidazole or a pyrazole catemers. Cyclic trimers of 1*H*-1,2,4-triazole (**1**), 3,5-dibromo-1*H*-1,2,4-triazole (**2**) (dbrtz), 3,5-dichloro-1*H*-1,2,4-triazole (**3**) (dcltz), dmpz (**4**), 4no2pz (**5**) and 4brpz (**6**).

in a Soxhlet apparatus with diethyl ether for 5 h. Compound **3b** was crystallized from benzene (m.p. by DSC 148.8 °C, lit.[15] m.p. 148 °C); yield, 0.144 g (46%).

NMR experiments

^{15}N cross-polarization magic angle spinning (CP/MAS) NMR experiments were performed using a Bruker MSL 300 (7.1 T) instrument at 300.13 MHz for ^{1}H and 30.41 MHz for ^{15}N and a 5 mm Varian/Chemagnetics standard high-speed CP/MAS probe. A Varian/Chemagnetics temperature unit was used to control the temperature of the cooling gas stream and a laboratory-built exchanger to achieve low temperatures. To avoid problems at low temperatures caused by air moisture, pure nitrogen obtained from evaporating liquid nitrogen was used as bearing, driving and cooling gas. All chemical shifts are related to external $^{15}NH_4Cl$ and given with an error of 0.3 ppm. CP/MAS spectra were measured using the usual CP pulse sequence[16] with a 6–10 ms ^{1}H 90° pulse width, 3–6 ms contact pulses and a 3–6 s recycle delay; the number of FIDs was between 100 and 500. The rotational frequencies were of about 6 kHz. ^{15}N-labelled tetramethyldibenzotetraaza[14]annulene (TTAA) in a separate capsule was used to calibrate the internal temperature of the samples inside the rotor.[9a,17] The ^{15}N chemical shifts were obtained using external polycrystalline $^{15}NH_4Cl$ as reference. In order to convert these data into the nitromethane scale, we used the relation[18]

$$\delta(CH_3NO_2) = \delta(^{15}NH_4Cl_{cryst}) - 338.1\,\text{ppm} \quad (1)$$

This equation differs from the relation

$$\delta(CH_3NO_2) = \delta(^{15}NH_4Cl_{liq}) - 352.9\,\text{ppm} \quad (2)$$

where $^{15}NH_4Cl_{liq}$ refers to a saturated solution of $^{15}NH_4Cl$ in D_2O at 298 K.[18] The difference $^{15}NH_4Cl_{cryst} - {}^{15}NH_4Cl_{liq} = 17.2$ ppm arises from different intermolecular interactions. Because of the larger chemical shift error in the nitromethane scale we use in this study the solid ammonium chloride scale, and give the values in the nitromethane scale calculated using Eqn (1).

Ab initio calculations

The calculations and drawings were carried out with the Xtal[19] and Gaussian 94[20] set of programs running on a DEC3000-300X workstation.

RESULTS AND DISCUSSION

Syntheses

We prepared 3,5-dibromo-1*H*-1,2,4-triazole (**2a**) and 3,5-dichloro-1*H*-1,2,4-triazole (**3a**) and the corresponding isotopologs **2b** and **3b** doubly labelled with ^{15}N at the adjacent positions N1 and N2 according to the route depicted in Fig. 2 (see Experimental section).

Crystallographic structures and structures calculated using *ab initio* methods

In order to discuss the crystal structures of the triazoles studied by NMR, the relevant intra- and intermolecular parameters for **3**[8] and **2**[6] were retrieved from the Cambridge Structural Database[21] (VITRUL and NABVIV, respectively, October 1999 release, CSD-O99 hereafter) and are assembled in Table 1. The average values for structures containing substituted triazole rings both at C3 and C5 ($R < 0.10$, no metals and no rings fused to the triazole) retrieved from CSD-O99 and the values for **1** as determined by x-ray analysis (TRAZOL01)[3] and by neutron diffraction at 15 K (TRAZOL04)[4] are included.

The values of the average bond angles for the 17 reported structures (21 fragments) excluding VITRUL show no significant differences from those reported by Goldstein *et al.* in 1969.[3] The angles at C3 and C5 show larger values of the standard deviations of the sample (in parentheses), probably owing to the electronic properties of the substituents that open and close these angles depending on the withdrawing and donating character of the substituents.[22]

The bond angles at N1 and N2 are sensitive to the position of the tautomeric H atom, opening the angle of the nitrogen to which it is bonded as reflected by the values for 1*H*-1,2,4-triazole itself and other 1*H* derivatives (C5—N1—N2 > N1—N2—C3, Table 1). This relationship, also supported by the *ab initio* calculations, is of great help in cases where the hydrogen atom could not be properly obtained from difference synthesis (the difficulty of locating H atoms by x-ray analysis is well known, even more so if these atoms are disordered). In **1** and 1*H*-unsubstituted analogues, either experimentally or *ab initio* calculated, the ring appears to be asymmetric as far as bond angles are concerned.

Averaging of the internal bond angles, by either static or dynamic disorder, is often encountered in NH-pyrazoles.[23] The ring in the VITRUL derivative **3a** is symmetric, showing a binary axis passing through N4 and the midpoint of the N1—N2 bond, probably resulting from proton disorder (occupancy factors of the disordered atoms close to 50%), although, as reported, electron density was only found close to N1.[8] In addition, the bond angles of the other reported 3,5-dichlorotriazole bearing a *p*-nitrophenyl group at N1 (SORBIK)[24] are similar to those considered typical for a non-disordered ring. In the 3,5-dibromo derivative NABVIV **2a**, which is

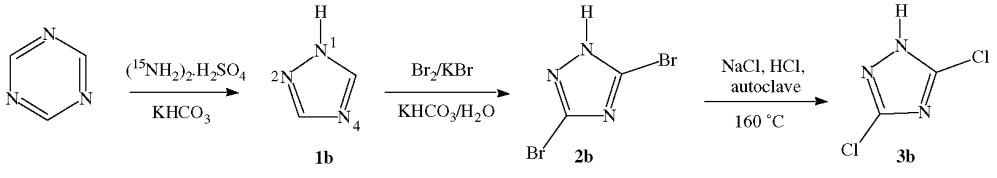

Figure 2. Synthetic scheme for the preparation of derivatives **2** and **3**.

Table 1. Selected geometrical parameters (Å, °)[a]

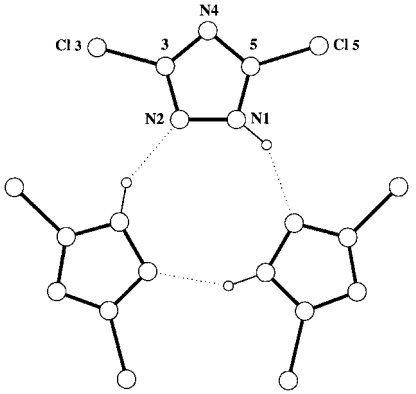

Parameter	VITRUL **3**	NANVIV **2**	SORBIK	TRAZOL01 **1**[3]	TRAZOL04 **1**[4]	Goldstein *et al.*[3]	CSD-O99	HF/6−311G** **1**	HF/6−311G** **1**[5]	HF/6−311G** **3**
C5—N1—N2	104.7 (3)	101.4 (14)	107.8 (3)	110.2 (2)	110.19 (4)	108.6 (8)	110.2 (8)	109.8	109.75	109.2
N1—N2—C3	105.3 (6)	105.3 (11)	101.3 (3)	102.1 (2)	102.67 (4)	101.8 (12)	101.3 (10)	102.5	102.48	101.9
N2—C3—N4	114.5 (4)	111.9 (12)	116.8 (4)	114.6 (2)	114.27 (5)	115.8 (9)	116.6 (19)	115.0	114.90	116.0
C3—N4—C5	100.6 (5)	102.7 (13)	101.7 (3)	103.0 (2)	102.90 (4)	103.2 (5)	102.2 (12)	102.5	102.49	101.6
N4—C5—N1	114.8 (5)	118.8 (11)	112.4 (4)	110.1 (2)	109.97 (5)	110.7 (6)	109.7 (13)	110.3	110.38	111.3
N2—N1—H1/R[1]	139 (3)	126 (−)	119.0 (3)	123 (1)	119.76 (9)	—	120 (4)	120.7	120.91	121.4
C5—N1—H1/R[1]	115 (2)	133 (−)	132.6 (4)	126 (1)	129.89 (9)	—	129 (4)	129.5	129.34	129.4
N···N	2.828 (4)	2.857 (28)	—	2.822 (3)	2.8117 (12)	—	—	—	—	—
N—H	0.94 (2)	1.00 (−)	—	1.04 (2)	1.0478 (14)	—	0.92 (9)	0.99	0.9884	0.99
H···N	1.96 (4)	1.85 (−)	—	1.82 (2)	1.7818 (12)	—	—	—	—	—
N—H···N	165 (2)	177 (−)	—	161 (2)	168.21 (16)	—	—	—	—	—

[a] The trimeric association of 3,5-dichloro-1*H*-1,2,4-triazole **3** (CSD refcode VITRUL) has been included to illustrate the numbering system. In SORBIK, R^1 = *p*-nitrophenyl, otherwise R^1 = H. A dash means that the NH hydrogen atom position was not refined.

pseudoisomorphous with VITRUL **3a**, the bond pattern is distorted from the usual values (Table 1), suggesting partial proton disorder and hence the reported H position[6] should correspond to the one with a lower occupancy factor.

In the *ab initio* calculations, several angular distortions are observed on comparing the bond angles of **1** and **3** (Table 1). These distortions, governed by the electronic properties of the substituents, follow the same qualitative trends as in benzenes,[22] i.e. the chlorine atom opens the *ipso* angle and closes the adjacent ones by 1.0° and −0.8° (Table 1) versus 1.9° and −1.4° in benzenes.[22]

Figures 3 and 4 illustrate the crystal packing of **1** (TRAZOL01) and **3a** (VITRUL), respectively (**2a**, NABVIV, is pseudoisomorphous with **3a**). Two hydrogen bond motives are observed as far as the N—H···N interactions are concerned. The molecules in **1** are arranged in chains parallel to their *a* axis [Fig. 3(a)] via N1—H1···N4 $(1/2 + x, y, -1/2 - z)$ hydrogen bonds (Table 1) and the chains, connected by C5—H5···N2 $(-x, 1/2 + y, 1/2 - z)$ contacts, form corrugated sheets [Fig. 3(b)] parallel to the *ab* plane [H5···N2, C5···N2, C5—H5···N2 = 2.48(2), 3.301(3) Å, 130(2)°] and the distance between them is $c/2 = 4.49$ Å. In VITRUL, the molecules are arranged in planar trimers [Fig. 4(a) and (b)] through hydrogen bonds in which contiguous nitrogen atoms are involved: N1—H1···N2 $(1 - x + y, 1 - x, 1/2 - z)$ (Table 1). The trimers lie in planes parallel to the *ab* plane without any hydrogen interactions between them. The distance between the planes of the trimers, $c/2 = 3.33$ Å, is shorter than in the parent compound. There are no significant differences either between the N···N distances in **2a** and **3a** or between the parent compound **1** and **3a**.

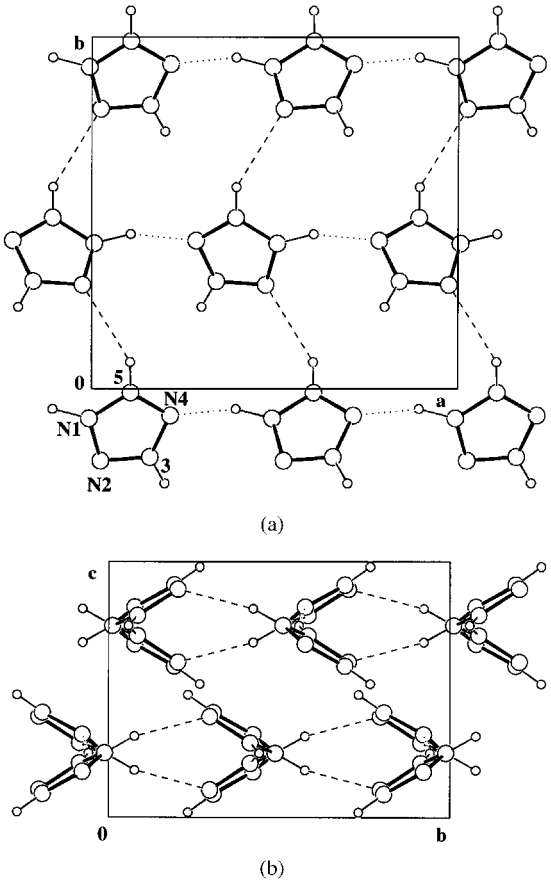

Figure 3. Secondary structure of 1*H*-1,2,4-triazole (CSD refcode: TRAZOL01) showing (a) the atomic numbering scheme and the packing of molecules in sheets parallel to the *ab* plane and (b) the packing of sheets along the *a* axis. The atoms are shown as spheres of arbitrary radii and dotted and dashed lines represent N—H···N and C—H···N hydrogen interactions, respectively.

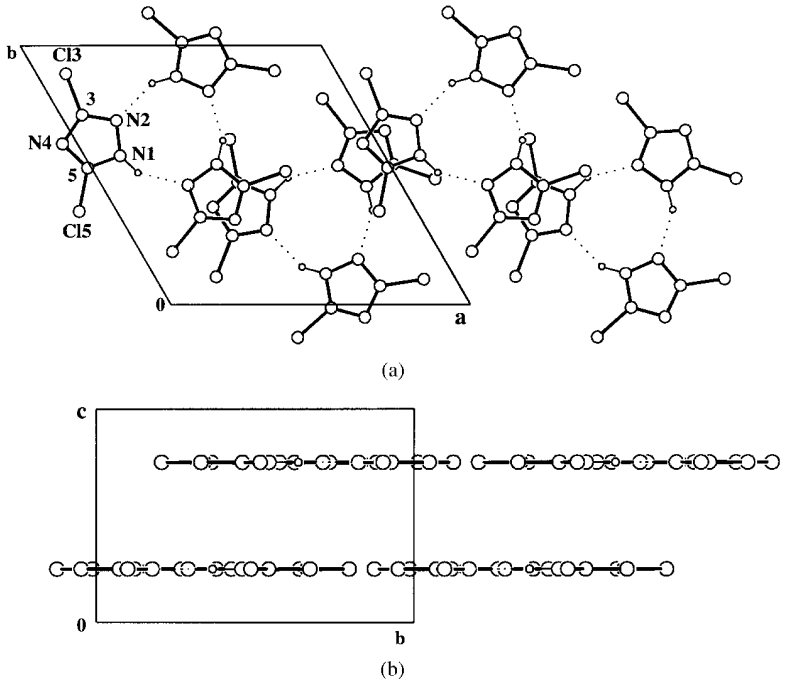

Figure 4. Secondary structure of 3,5-dichloro-1*H*-1,2,4-triazole (**3**) (CSD refcode: VITRUL) showing (a) the atomic numbering scheme and the arrangement of molecules in trimers down the *c* axis and (b) the packing of trimers along the *a* axis. The atoms are shown as spheres of arbitrary radii and dotted lines represent N—H···N hydrogen bonds.

In summary, and considering the influence of the substituents, either from a crystallographic or a quantum chemical analysis the bond angles pattern suggests a complete proton disorder (50 : 50) for the 3,5-dichloro-derivative **3a** whereas the 3,5-dibromo-1*H*-1,2,4-triazole (**2a**) is only partially disordered. In addition, both compounds form a cyclic hydrogen bond motif, which, as in pyrazoles,[25] is the necessary condition for proton transfer in the solid state from N1 to N2 and vice versa.

Examination of Table 1 shows that N2—N1—H1 = 120° and C5—N1—H1 = 130° (TRAZOL04, CSD-O99 and all calculations). SORBIK, an N1-substituted compound, also obeys that rule, but TRAZOL01 is distorted, showing that the protons have not been localized correctly. The case of the dichloro derivative, VITRUL (139 and 115°), is totally inconsistent whereas the dibromo derivative, NANVIV (126 and 133°), is more normal. We carried a number of calculations (Table 2) to determine the percentages of disorder, either dynamic or static, from the internal angles at N1 (C5—N1—N2) and N2 (N1—N2—C3). The results concerning VITRUL **3a** indicate to a mixture of 1*H*- and 2*H*-tautomers in a 45 : 55 ratio. Note that the less populated tautomer corresponds to the localized proton. The results concerning NANVIV **2a** cannot be properly analyzed even considering that the proton has probably been localized on the less populated tautomer.

Variable-temperature solid-state ^{15}N NMR spectroscopy

Figure 5 depicts the superposed experimental and calculated ^{15}N CP/MAS NMR spectra of dbrtz (**2b**) and of dcltz (**3b**). For comparison we also show the corresponding spectra of dmpz (**4**) adapted from Ref. 10. All spectra contain the four sharp lines of TTAA added in order to obtain the sample temperature using the calibration data of Ref. 17. All spectral parameters, rate and equilibrium constants determining the lineshapes are given in Table 3 and the intrinsic nitrogen chemical shifts in Table 4.

At low temperatures, all compounds give rise to a high-frequency line arising from the imino nitrogen N2 and a low-frequency line arising from the amino nitrogen N1. The line splitting corresponds to the intrinsic splitting $\Delta\nu = \delta(\text{—}N\text{=}) - \delta(\text{NH}) \times 30.41 \times 10^6$ Hz. As temperature is raised the lines of dmpz and dcltz broaden and coalesce. Whereas only a single averaged line is observed for dmpz, two lines with a high-temperature splitting of $\delta\nu < \Delta\nu$ is observed for dcltz. As shown before,[17,27] these findings indicate a degenerate proton tautomerism in dmpz but a non-degenerate process in dcltz, where the equilibrium constant is given by

$$K = k_{12}/k_{21} = x_2/x_1 = (1 - \delta\nu/\Delta\nu)/(1 + \delta\nu/\Delta\nu) \quad (3)$$

In other words, $K = 1$ in the case of dmpz but $K < 1$ in the case of dcltz. The $\delta\nu$ values of the latter decrease with increasing temperature as K increases.

K was obtained from $\delta\nu$ and $\Delta\nu$ at high temperatures using Eqn (3). The low-temperature values were then obtained from the high-temperature values by extrapolation using the van't Hoff equation. The values of the intrinsic linewidth W_0 were determined at high and low temperatures by lineshape analysis. For dcltz (**3b**), a single constant value of $W_0 = 150$ Hz was employed to simulate the spectra in the whole temperature range. In the case of dbrtz (**2b**) a large value, $W_0 = 300$ Hz, had to be used. These values are much larger than those found previously[10] for dmpz [Fig. 5(a)]. The origin of this effect could not be determined in this study and prevented the determination of rate constants of the triple proton transfer in a large temperature range by lineshape analysis. For similar reasons we performed additional magnetization transfer experiments in the case of dmpz in order to obtain rate constants in a large temperature range. Such experiments could not be performed in this study, however, as they require singly ^{15}N-labelled materials where spin diffusion artifacts are suppressed.[10] For the discussion of the kinetic parameters of dcltz we therefore consider only the values obtained in the usual way around the coalescence point around 210 K by lineshape analysis.[27]

The case of dbrtz is similar to that of dcltz, but the intrinsic linewidths are even larger. Strong lineshape

Table 2. Interpolation results[a]

		1 (x-ray)		**1** (neutron)		**1** (6–31G*)		**1** (6–311G**)		**3** (6–31G**)	
Compound	Method	N1	N2	N1	N2	N1	N2	N1	N2	N1	N2
1	X-ray	**100.0**	**0.0**	100.1	−7.6	105.5	−5.5	106.2	−5.2	113.7	2.7
1	Neutron	99.9	7.0	**100.0**	**0.0**	105.3	2.3	106.1	2.6	113.6	10.5
1	6–31G**	95.1	4.9	94.8	−2.3	**100.0**	**0.0**	100.7	−0.3	108.2	8.2
1	6–311G**	94.4	4.7	94.1	−2.5	99.3	−0.3	**100.0**	**0.0**	107.5	7.9
X-ray	32.1	39.5	27.0	35.0	30.1	38.4	30.5	38.8	38.4	46.6	
3	6–31G**	87.7	−2.5	86.8	−10.2	91.8	−8.2	92.4	−8.0	**100.0**	**0.0**
2	X-ray	−8.6	39.5	−16.9	35.0	−15.1	38.4	−14.9	38.4	−6.8	46.6
2	X-ray (inv)	39.5	−8.6	35.0	−16.9	38.4	−15.1	38.8	−14.9	46.6	−6.8

[a] The interpolation equations used are as follows: % tautomer using the angle on N1 = 100 ([C5—N1—N2] – [**N1—N2—C5**]/[**C5—N1—N2**] – [**N1—N2—C3**]) and % tautomer using the angle on N2 = 100 ([N1—N2—C3] – [**N1—N2—C5**]/[**C5—N1—N2**] – [**N1—N2—C3**]). In bold are the angles corresponding to the method used for the interpolations.

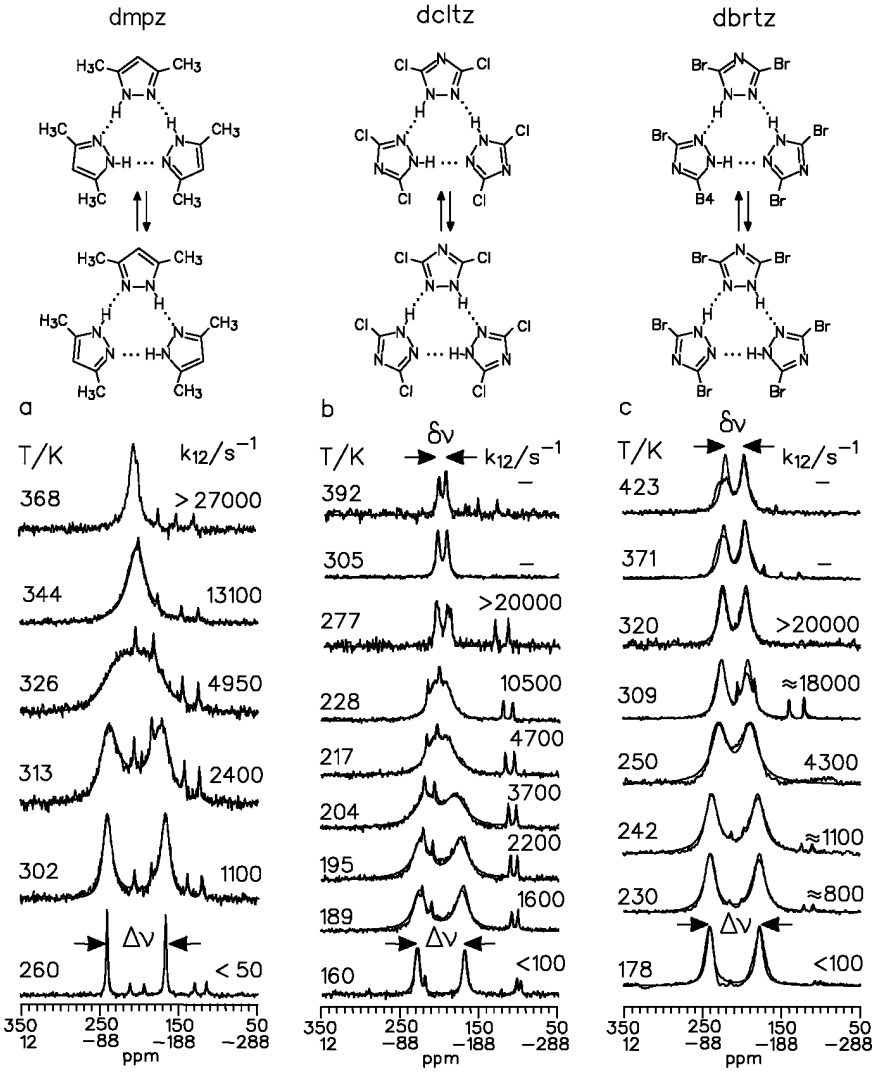

Figure 5. Superposed experimental and calculated 30.41 MHz ^{15}N CP/MAS NMR spectra of 95% ^{15}N-enriched dmpz (adapted from Ref. 10), dcltz and dbrtz as a function of the temperature. Upper chemical shift values, reference solid $^{15}NH_4Cl$; lower values, reference liquid CH_3NO_2. The sharp lines with strongly temperature-dependent line positions stem from TTAA (tetramethyldibenzotetraaza[14]annulene-$^{15}N_4$) or 1,8-dihydro-5,7,12,14-tetramethyldibenzo(b,i)-$^{15}N_4$-(1,4,8,11)-tetraazacyclotetradeca-4,6,11,13-tetraene) added in small portions. The sample temperature was determined from the TTAA line positions by simulation according to Ref. 10.

changes are observed between 240 and 250 K. At high temperatures a splitting $\delta\nu$ was also obtained by lineshape analysis. However, the two lines at room temperature exhibit remarkedly different widths, and at higher temperatures sharp features revealing further dynamic processes or phenomena whose origin could not yet be analysed in this study. They might be tentatively assigned to residual dipolar couplings to bromine.[28] Similar non-resolved couplings to chlorine may also lead to the large linewidth of dcltz. Anyway, in the case of dbrtz we only take the rate constants k_{12} determined by lineshape simulation around 250 K into account.

Discussion of the kinetic results

In Fig. 6 we have plotted the rate constants k_{12} of dcltz and dbrtz in an Arrhenius diagram as a function of the inverse temperature. From a linear least-squares fitting we obtain activation energies 21 and 19 kJ mol^{-1} and the pre-exponential factors $10^{8.2}$ and $10^{7.2}$ s^{-1}. In view of the limited temperature range and the limitations of the lineshape method, these values are subject to a large unknown margin of error. Nevertheless, they seem to indicate frequency factors which are much smaller than the usual value of $10^{12}-10^{13}$ s^{-1} found for solid-state proton transfer of other azoles.[10] On the other hand, the few rate constants obtained which seem to be reliable allow a comparison with the kinetic data of the three pyrazole included in Fig. 6. For the sake of clarity only the calculated rate constants are shown, taken from Refs 10 and 11. The rate constants of the pyrazoles exhibit strongly a non-Arrhenius behaviour as depicted in Fig. 6. The temperature dependence was calculated by non-linear least-squares data fitting to the experimental rate constants using a modified Bell tunnelling model

described previously,[10,11,29] based on a more or less concerted triple proton transfer process involving a single barrier. These curves depend on the following parameters:

(i) E_m represents a minimum energy for tunnelling to occur. It represents a contribution arising from heavy atom reorganization *preceding* the hydron tunnelling process at $T = 0$;
(ii) E_d is the barrier height for the triple proton transfer;
(iii) $2a$ is the barrier width of the H transfer in Å at energy E_m;
(iv) a single frequency factor A (in s^{-1}) is used which is allowed to vary between 10^{12} and 10^{13} s^{-1};
(v) the tunnelling masses are given in the stepwise case by $m_{eff} = 3 + \Delta m$, where the first term represents the mass of three moving protons and the second is an additional term representing heavy atom reorganization during the tunnelling process.

Table 3. Results of the ^{15}N CP/MAS lineshape analysis of dbrtz (**2b**) and dcltz (**3b**)[a]

dbrtz (**2b**)			dcltz (**3b**)		
T (K)	K	k_{12}	T (K)	K	k_{12}
423	0.43	—	392	0.75	—
371	0.39	—	356	0.72	—
320	0.37	>20 000	305	0.69	—
309	0.36[b]	~18000	284	0.68	—
250	0.31[b]	4300	277	0.67	—
242	0.30[b]	1100	268	0.66	—
230	0.29[b]	~800	256	0.65[b]	—
210	0.27[b]	~350	248	0.64[b]	>20000
208	0.26[b]	~300	239	0.63[b]	~20000
203	0.26[b]	~200	228	0.62[b]	10500
200	0.25[b]	~170	217	0.61[b]	4700
178	0.23[b]	~100	209	0.60[b]	4500
			204	0.59[b]	3700
			199	0.58[b]	2700
			195	0.57[b]	2200
			189	0.56[b]	1600
			160	0.52[b]	<100

[a] K = equilibrium constant; k_{12} = rate constant of proton tautomerism as defined in Eqn (3).
[b] Extrapolated values from high temperature using the van't Hoff equation. Further parameters of the lineshape analysis: $W_0 = 300$ Hz for **2b**; $W_0 = 150$ Hz for **3b** constant over the whole temperature range.

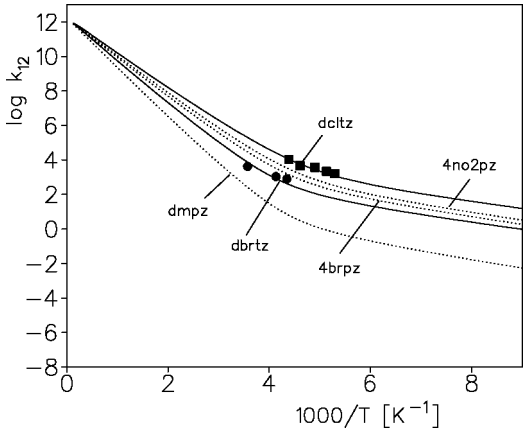

Figure 6. Arrhenius diagram of the triple proton transfer in dcltz and dbrtz. For comparison the calculated Arrhenius curves of the corresponding processes in dmpz, 4no2pz and 4brpz published in Ref. 11 are also shown.

We note that the kinetic data obtained here for dcltz and dbrtz exhibit a very similar behaviour to those obtained previously for 4no2pz and 4brpz, but the kinetics are substantially faster than in the case of dmpz. In other words, as far as the triple proton transfer characteristics are concerned, triazoles and pyrazoles can be discussed in terms of a related series of molecules. This finding assists us to construct the temperature dependence of the rate constants of triple proton transfer in the triazole cases by taking most tunnelling parameters from the pyrazole series. Only E_m and E_d were varied slightly. The results are given in Table 5. Naturally, the temperature dependence proposed should be confirmed by additional experiments.

In order to evaluate the different proton transfer

Table 5. Molecular and dynamic properties of compounds **2–6**[a]

	E_d	E_m	$E_d + E_m$	Log A	Δm	$2a$
dbrtz (**2**)	42.0	7.1	49.1	12.3	2.8	0.43
dcltz (**3**)	33.5	6.7	40.2	12.3	2.8	0.43
dmpz (**4**)	48.1	8.4	56.5	12.3	2.8	0.43
4no2pz (**5**)	36.0	7.5	43.5	12.3	2.8	0.39
4brpz (**6**)	38.0	7.5	45.5	12.3	2.8	0.39

[a] Parameters of the modified Bell tunneling model: barrier height E_d and minimum energy for tunneling E_m in kJ mol^{-1}, barrier width $2a$ in Å, frequency factor A in s^{-1} (tunneling masses $m_{eff}^{HHH} = 3 + \Delta_m$).

Table 4. Intrinsic ^{15}N chemical shifts and hydrogen bond distances of triazoles, pyrazoles, porphyrin and porphycene in the solid state

	δ(—N=)[a]	δ(N—H)[a]	δ(—N=)[b]	δ(N—H)[b]	Δ	R(N···N) (Å)	R(NH) (Å)	R(H···N) (Å)
dbrtz (**2**)	240.5	177.3	−97.6	−160.8	63.2	2.86	1.045	1.825
dcltz (**3**)	227.8	168.6	−110.3	−169.5	60.5	2.83	1.055	1.775
dmpz (**4**)	241.3	166.8	−111.6	−186.1	74.5	2.98	1.04	1.94
4no2pz (**5**)	243.2	170.7	−109.7	−182.2	72.5	2.87	1.045	1.825
4brpz (**6**)	247.0	172.3	−105.9	−180.6	74.7	2.89	1.04	1.85
Porphyrin	215	107	−137.9	−245.9	108	2.89	1.03	2.28
Porphycene	187	135	−165.9	−217.9	46	2.63	1.10	1.60

[a] Reference: solid $^{15}NH_4Cl$; ppm values are given with a margin of error of ±0.3 ppm.
[b] Nitromethane scale $\delta(CH_3NO_2) = \delta(NH_4Cl) - 338.1$ ppm.[18]

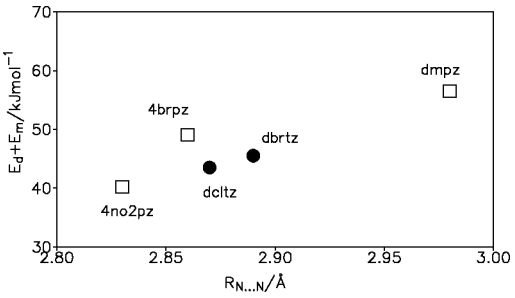

Figure 7. Sum of the minimum energy for tunneling to occur, E_m, and the barrier height, E_d, of concerted triple proton transfer processes in cyclic triazole and pyrazole trimers.

dynamics of the five compounds we have plotted in Fig. 7 the total barrier height $E_m + E_d$ as a function of the crystallographic N···N distances. We obtain a correlation which seems to be significant: when the N···N distances are increased because of substituent effects or crystal packing forces, the barrier height of proton transfer increases, a very plausible result.

If one assumes that the barriers are proportional to a parameter, the molar refractivity MR, which represents a mixture of steric and polarizability effects, then clearly pyrazoles and 1,2,4-triazoles belong to two different families. To have a common behaviour, it is necessary to make an additional hypothesis, that the replacement of C4-H (pyrazoles) by N4 (1,2,4-triazoles) decreases both E_d (14.8 kJ mol^{-1}) and E_m (1.9 kJ mol^{-1}).

For the five compounds in Table 5 (**2**, MR = 0.60; **3**, MR = 0.89; **4**, MR = 0.56; **5** and **6**, MR = 0.10) we have

$$E_d = (34.4 \pm 0.8) + (24.6 \pm 1.5)\text{MR}, R^2 = 0.989$$

$$E_m = (7.3 \pm 0.1) + (2.0 \pm 0.1)\text{MR}, R^2 = 0.991$$

$$E_d + E_m = (41.7 \pm 0.8) + (26.5 \pm 1.4)\text{MR}, R^2 = 0.992$$

Discussion of hydrogen bond geometry and ^{15}N chemical shifts

In this section we will discuss how well the compounds studied here fit into the well-known hydrogen bond geometry correlation of N—H···N hydrogen bonds proposed on the basis of neutron structures by Steiner and Saenger[30a,b] and Gilli *et al.*[30c] and from NMR and theoretical data.[31,32] This correlation for the two N—H and the H···N distances r_1 and r_2 can be written as

$$r_2 = r_0 - b\ln[1 - \exp[-(r_1 - r_0)/b]] \qquad (4)$$

with $b = 0.404$ Å and $r_0 = 0.99$ Å. This hydrogen bond correlation can also be written as a correlation between the two coordinates $q_2 = r_1 + r_2$ and $q_1 = 1/2(r_1 - r_2)$, where q_2 represents the N···N distance in the case of a linear hydrogen bond and q_1 the average distance of the proton to the hydrogen bond center. From Eqn (4), it follows that

$$q_2 = 2r_0 + 2q_1 + 2b\ln[1 + \exp(-2q_1/b)] \qquad (5)$$

with $b = 0.404$ Å and $r_0 = 0.997$ Å.

In Fig. 8(a) we have plotted the correlation curve q_2 as a function of q_1 according to Eqn (5) as a solid line, together with the values for pyrazole and triazole trimers, together with values taken from Ref. 11 for porphyrin and porphycene. Each pair of circles at a given value of q_2 indicates the two quasi-degenerate tautomeric states between which the proton transfer occur. The correlation line is a crude guideline of the two-dimensional minimum reaction energy pathway. This pathway will consist of a combination of a hydrogen bond compression, i.e. the motion along the correlation line, and actual proton transfer at a constant reduced q_2 value. The experimental data points were obtained as follows. Assuming that all hydrogen bonds are quasi-linear in the case of the triazoles and pyrazoles, we can take the crystallographic N···N distances as approximations for q_2. Then we calculate q_1 by solving Eqn (5) for each point. Naturally, the result is that all data points are located on the correlation curve in Fig. 8(a). In other words, using the correlation we estimate the N···H and H···N distances for the various compounds included in Table 5. For example, we obtain a value of 1.04 Å for the NH distance in dmpz, which compares well with the ND distance of 1.05 Å determined previously using dipolar solid-state ^{15}N NMR.[33] This indicates that the assumption of quasi-linear hydrogen bonds in dmpz is well fulfilled. For comparison, we have added the corresponding values of the non-linear hydrogen bonds of porphycene and porphyrin according to the analysis of Ref. 26.

Let us now ask whether and how the nitrogen chemical shifts reflect the hydrogen bond geometries. For this purpose we have plotted in Fig. 8(b) the N···H distance as a function of the nitrogen chemical shift for each compound. As proposed previously,[33] we express the nitrogen chemical shift in terms of the equation

$$\delta(^{15}\text{N}) = \delta_\infty - \Delta_0 \exp[-(r_1 - r_0)/b] \qquad (6)$$

where r_1 is the N···H distance, δ_∞ is the nitrogen chemical shift at very large N···H distances and $\delta_\infty - \Delta_0$ is the value of the chemical shift at $r_1 = r_0$. The calculated curves in Fig. 8(b) were obtained with the values $\delta_\infty = 260$ ppm and $\Delta_0 = 90$ ppm for the pyrazoles and triazoles and $\delta_\infty = 220$ ppm and $\Delta_0 = 120$ ppm for porphyrin and porphycene. It is clear that the nitrogen chemical shifts are both influenced by the chemical structure and by the hydrogen bond geometry. Only within a given series is it possible to associate the nitrogen chemical shift with changes of the hydrogen bond geometries alone.

By contrast, if we plot the intrinsic chemical shift differences between the protonated and the non-protonated nitrogen atoms we obtain the graph in Fig. 8(c). The solid line was calculated from Eqns (5) and (6). It is seen that is a better measure of the proton transfer coordinate q_1.

CONCLUSIONS

We have shown that substituted triazoles can form cyclic trimers in the solid state like suitably substituted pyrazoles in which degenerate or quasi-degenerate triple proton transfer takes place. The triple proton transfer kinetics

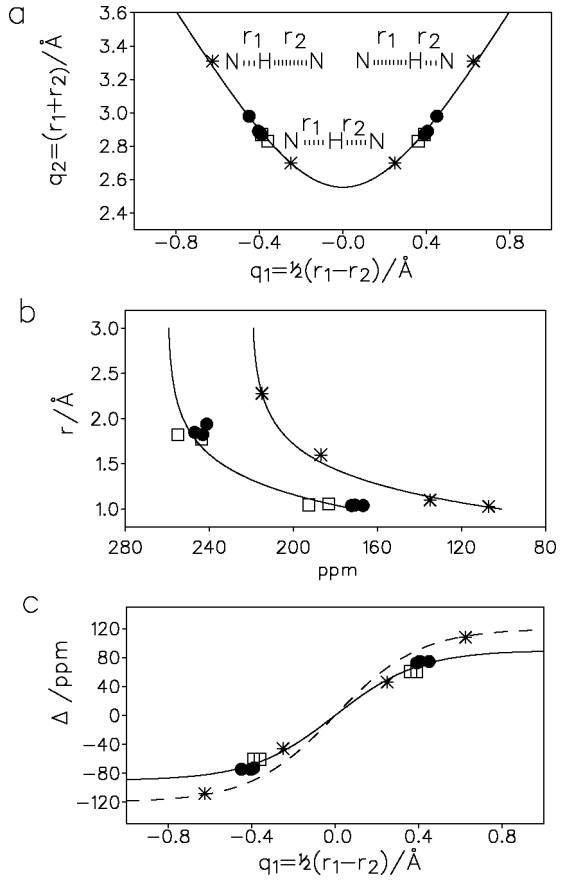

Figure 8. (a) Hydrogen bond correlation for triazoles (□), pyrazoles (●), porphyrin and porphycene (*). Data from this study and from Ref. 26. r_1 and r_2 represent the two N···H distances of the corresponding N—H···N hydrogen bonds, $q_1 = 1/2(r_1 - r_2)$ the proton transfer coordinate and $q_2 = r_1 + r_2$ the heavy atom coordinates. The solid line was calculated according to Eqn (5). (b) Dependence of the associated ^{15}N chemical shifts as a function of the N···H distance. Reference solid $^{15}NH_4Cl$. The solid line was calculated according to Eqns (5) and (6). (c) Intrinsic chemical shift difference of the two ^{15}N nuclei of the N—H···N units as a function of q_1. The solid line was calculated according to Eqns (5) and (6). For further information, see text.

are similar to those of the pyrazoles where a concerted triple proton transfer taking place at low temperatures by tunnelling has been established previously[10,11] by determining rate constants and multiple kinetic H/D isotope effects in a large temperature range. The tunnelling analysis shows a monotonic increase in the proton transfer barrier with increasing N···N hydrogen bond distances. The different chemical and crystallographic structure of the various pyrazoles and triazoles considered seems, therefore, to influence the proton transfer barrier only indirectly via a different hydrogen bond geometry rather than by direct electronic effects. Using the NH···N hydrogen bond geometry correlation established recently,[30–32] it is possible to derive N···H distances of the order of 1.05 Å which are in good agreement with those obtained by crystallography and dipolar NMR.[34] Finally, the intrinsic nitrogen chemical shifts of pyrazoles and triazoles are related roughly in a simple way to the hydrogen bond geometry.

Acknowledgements

This work was financed by the DGICYT (PB96-0001-C03) and Comunidad de Madrid (07N/0001/1999) of Spain, the Deutsche Forschungsgemeinschaft, Bonn Bad Godesberg, and the Fonds der Chemischen Industrie, Frankfurt. One of us (M.A.G.) thanks the UNED for a fellowship.

REFERENCES

1. Minkin V, Garnovskii AD, Elguero J, Denisko OV, Katritzky AR. In *Advances in Heterocyclic Chemistry*, vol. 76, Katritzky AR (ed.). Academic Press: London, 2000.
2. Deuschl H. *Ber. Bunsenges. Phys. Chem.* 1965; **69**: 550.
3. Goldstein P, Ladell J, Abowitz G. *Acta Crystallogr., Sect. B* 1969; **25**: 135.
4. Jeffrey GA, Ruble JR, Yates JH. *Acta Crystallogr., Sect. B* 1983; **39**: 388.
5. Fuhrmann P, Koritsánszky T, Luger P. *Z. Kristallogr.* 1997; **212**: 213.
6. Valkonen J, Pitkänen I, Pajunen A. *Acta Chem. Scand., Ser. A* 1985; **39**: 711.
7. Pitkänen I, Valkonen J, Pitkänen M. *Z. Kristallogr.* 1988; **185**: 243.
8. Starova GL, Frank-Kamenetskaya OV, Makarskii VV. *Kristallografiya* 1990; **35**: 449.
9. (a) Smith JAS, Wehrle B, Aguilar-Parrilla F, Limbach H-H, Foces-Foces C, Cano FH, Elguero J, Baldy A, Pierrot M, Khurshid MMT, Larcombe-McDouall JB. *J. Am. Chem. Soc.* 1989; **111**: 7304; (b) Aguilar-Parrilla F, Scherer G, Limbach H-H, Foces-Foces MC, Cano FH, Smith JAS, Toiron C, Elguero J. *J. Am. Chem. Soc.* 1992; **114**: 9657.
10. Aguilar-Parrilla F, Klein O, Elguero J, Limbach H-H. *Ber. Bunsenges. Phys. Chem.* 1997; **101**: 889, and references cited therein.
11. Klein O, Bonvehi MM, Aguilar-Parrilla F, Elguero J, Limbach H-H. *Isr. J. Chem.* 1999; **39**: 291.
12. Elguero J, Limbach H-H, Aguilar-Parrilla F, Claramunt RM, López C. *Nuevas Tendencias, Cristalografía*. CSIC: Madrid, 1995; 187.
13. Rowlett RS, Klysa T, Shiraki WW. *J. Label. Compd. Radiopharm.* 1990; **28**: 1437.
14. Grinshtein VYa, Strazdin AA. *Khim. Geterotsikl. Soedin.* 1969; **5**: 1114.
15. Miethchen R, Seipt H-U, Kröger C-F. *Z. Chem.* 1969; **9**: 300.
16. Torchia D. *J. Magn. Reson.* 1978; **30**: 613.
17. Wehrle B, Aguilar-Parrilla F, Limbach H-H. *J. Magn. Reson.* 1990; **87**: 584.
18. (a) Witanowski M, Stefaniak L, Szymanski S, Januszewski H. *J. Magn. Reson.* 1977; **28**: 217; (b) Witanowski M, Stefaniak L, Webb GA. *Annu. Repo. NMR Spectrosco.* 1981; **11B**; (c) Martin G, Martin ML, Gouesnard JP. *NMR—Basic Principles and Progress, Vol. 18, ^{15}N NMR Spectroscopy*. Springer: Heidelberg, 1989; (d) Srinivasan PR, Lichter RL. *J. Magn. Reson.* 1977; **28**: 227; (e) Claramunt RM, Sanz D, López, C, Jiménez JA, Jimeno ML, Elguero J, Fruchier A. *Magn. Reson. Chem.* 1997; **35**: 35.
19. Hall SR, Flack HD, Stewart JM. *Xtal3.2*. University of Western Australia: Lamb, Perth, 1994.
20. Frisch MJ, Trucks GM, Schlegel HB, Gill MWP, Johnson BG, Robb MA, Cheeseman JR, Keith T, Peterson GA, Montgomery JA, Raghavachari K, Al-Laham MA, Zakrzewski VG, Ortiz JV, Foresman JB, Cioslowski J, Stefanov BB, Nanayakkara A, Challcombe M, Peng CY, Ayala PY, Cheng W, Wong W, Andres JL, Replogle ES, Gomperts R, Martin RL, Fox DJ, Binkley JS, Defrees DJ, Baker J, Setwart JP, Head-Gordon M, Gonzalez C, Pople JA. *Gaussian 94*. Gaussian: Pittsbugh, PA, 1995.
21. Allen FH, Davies JE, Galloy JJ, Johnson O, Kennard O, Macrae CF, Mitchell EM, Mitchell JF, Smith JM, Watson DG. *J. Chem. Inf. Comput. Sci.* 1991; **31**: 187.
22. Domenicano A, Murray-Rust P. *Tetrahedron Lett.* 1979; **24**: 2283.
23. Llamas-Saiz AL, Foces-Foces C, Fontenas C, Jagerovic N, Elguero J. *J. Mol. Struct.* 1999; **484**: 197, and references cited therein.
24. Ishihara M, Tonogaki M, Ohba S, Saito Y, Okazaki M, Katoh T, Kamiyama K. *Acta Crystallogr., Sect. C* 1992; **48**: 184.

25. Elguero J, Cano FH, Foces-Foces C, Llamas-Saiz AL, Limbach H-H, Aguilar-Parrilla F, Claramunt RM, López C. *J. Heterocycl. Chem.* 1994; **31**: 695.
26. Langer U, Hoelger Ch, Wehrle B, Latanowicz L, Vogel E, Limbach H-H. *J. Phys. Org. Chem.* 2000; **13**: 23.
27. Limbach H-H, Hennig J, Kendrick RD, Yannoni CS. *J. Am. Chem. Soc.* 1984; **106**: 4059.
28. Harris RK, Olivieri AC. *Prog. Nucl. Magn. Reson. Spectrosc.* 1992; **24**: 435.
29. (a) Bell RP. *The Tunnel Effect*. (2nd edn). Chapman and Hall: London, 1980; (b) Caldin E, Gold V. *Proton Transfer*. Chapman and Hall: London, 1975.
30. (a) Steiner Th, Saenger W. *Acta Crystallogr., Sect. B* 1994; **50**: 348; (b) Steiner Th. *J. Chem. Soc., Chem. Commun.* 1995; 1331; (c) Gilli P, Bertolasi V, Ferretti V, Gilli G. *J. Am. Chem. Soc.* 1994; **116**: 909.
31. Benedict H, Limbach H-H, Wehlan M, Fehlhammer WP, Golubev NS, Janoschek R. *J. Am. Chem. Soc.* 1998; **120**: 2939.
32. Alkorta I, Rozas I, Elguero J. *Struct. Chem.* 1998; **9**: 243.
33. Smirnov SN, Benedict H, Golubev NS, Denisov GS, Kreevoy MM, Schowen RL, Limbach H-H. *Can. J. Chem.* 1999; **77**: 943.
34. Hoelger CG, Limbach H-H, Aguilar-Parrilla F, Elguero J, Weintraub O, Vega S. *J. Magn. Reson. A* 1996; **120**: 46.

